Neuron, Vol. 41, 745–754, March 4, 2004, Copyright ©2004 by Cell Press

Identification of the Components Controlling Inactivation of Voltage-Gated Ca^{2+} Channels

James Kim,[1] Smita Ghosh,[1] Deborah A. Nunziato,[1] and Geoffrey S. Pitt[1,2,*]
[1]Department of Pharmacology
[2]Department of Medicine
Division of Cardiology
College of Physicians and Surgeons
of Columbia University
630 West 168th Street, PH 7W 318
New York, New York 10032

Summary

Ca^{2+}-dependent inactivation (CDI) of L-type voltage-gated Ca^{2+} channels limits Ca^{2+} entry into neurons, thereby regulating numerous cellular events. Here we present the isolation and purification of the Ca^{2+}-sensor complex, consisting of calmodulin (CaM) and part of the channel's pore-forming α_{1C} subunit, and demonstrate the Ca^{2+}-dependent conformational shift that underlies inactivation. Dominant-negative CaM mutants that prevent CDI block the sensor's Ca^{2+}-dependent conformational change. We show how Ile1654 in the CaM binding IQ motif of α_{1C} forms the link between the Ca^{2+} sensor and the downstream inactivation machinery, using the α_{1C} EF hand motif as a signal transducer to activate the putative pore-occluder, the α_{1C} I-II intracellular linker.

Introduction

Ca^{2+} entry through members of the family of neuronal high voltage-activated calcium channels is limited by Ca^{2+}-dependent inactivation (CDI), a process that depends on constitutively bound CaM (Liang et al., 2003). This obligate channel subunit forms part of the Ca^{2+} sensor that triggers inactivation and thereby controls many neuronal processes regulated by Ca^{2+}, such as gene expression and synaptic vesicle release, at the point of Ca^{2+} influx. Since CDI is most prominent in L-type ($Ca_V1.2$) Ca^{2+} channels, dissection of its molecular mechanisms has guided much of this work (Budde et al., 2002).

A major part of this effort has been attempts to understand how CaM and the channel form the Ca^{2+}-sensing apparatus. Components in the channel include an IQ motif (IQ) in the C terminus of the pore-forming α_{1C} subunit (Zühlke and Reuter, 1998) that acts as a Ca^{2+}/CaM effector site (Peterson et al., 1999; Zühlke et al., 1999) and a putative EF hand (EF), located more proximal in the C terminus (Babitch, 1990). EF was originally suggested as the Ca^{2+} binding site (de Leon et al., 1995), but subsequent studies ruled this out (Zhou et al., 1997), suggesting instead that EF contributes to the downstream signal transduction process (Peterson et al., 2000). EF may also regulate voltage-dependent inactivation (VDI) (Bernatchez et al., 1998). Studies with Ca^{2+}-insensitive CaM mutants (Peterson et al., 1999; Zühlke et al., 1999), which acted as dominant negatives, highlighted that α_{1C} must also harbor an apoCaM binding site. A variety of biochemical (Mouton et al., 2001; Pate et al., 2000; Pitt et al., 2001; Romanin et al., 2000) and imaging (Erickson et al., 2003) techniques pinpointed a $\sim$110 amino acid domain between EF and IQ, although the details of apoCaM interaction remain controversial.

Three smaller regions within this domain have received particular attention based on their ability to interact with CaM in low [Ca^{2+}] or with Ca^{2+}-insensitive CaM mutants (Figure 1). Most amino-terminal is the region surrounding amino acids 1588–1609, labeled peptide A (Pitt et al., 2001) or LM1 (Romanin et al., 2000), which can bind to CaM in the absence of Ca^{2+}. The second region, labeled peptide C (Pitt et al., 2001) or CB (Pate et al., 2000), binds CaM with a $k_{1/2}$ for Ca^{2+} of $<$90 nM (Pitt et al., 2001), can form a ternary complex with CaM and the IQ motif (Mouton et al., 2001), and contains determinants necessary for interaction with a Ca^{2+}-insensitive CaM mutant (Erickson et al., 2003). Finally, two-hybrid FRET analysis has shown that a sequence surrounding the IQ motif can also interact with a mutant CaM (Erickson et al., 2003). Together, these studies support a model in which noncontiguous sequences in this proximal portion of the α_{1C} C terminus form the apoCaM tethering site (Erickson et al., 2003; Pitt et al., 2001). The specific boundaries of the apoCaM interaction site remain controversial, however, preventing a molecular understanding of how CaM forms the Ca^{2+} sensor apparatus and how it participates in gating of Ca^{2+} channels.

Not only how these components form a Ca^{2+} sensor but also how the sensor triggers channel inactivation remain unknown. Understanding this process would reveal important insights not only into CDI but also into the general mechanism of Ca^{2+} channel gating, since several reports have suggested that CDI and VDI utilize the same machinery, with the α_{1C} cytoplasmic I-II linker forming a blocking particle as the common endpoint (Cens et al., 1999; Stotz et al., 2000). Where these pathways intersect is unclear, but common components may include not only EF (Bernatchez et al., 1998), but also CaM and its interaction sites in the α_{1C} C terminus, since apoCaM and/or the apoCaM tethering site(s) have been suggested as regulators of VDI (Pitt et al., 2001). Although a recent report supports this role for apoCaM tethering (Erickson et al., 2003), definitive proof for this model is lacking, as apoCaM tethering sites outside of the multifunctional IQ have not been tested.

Here we report the in vitro isolation and purification of the Ca^{2+} sensor and signal transduction apparatus responsible for inactivation, a complex between CaM and the proximal portion of the α_{1C} C terminus. We show that the sensor undergoes Ca^{2+}-dependent conformational changes that predict CDI. Using this complex to probe apoCaM interaction, we also demonstrate how CaM and the α_{1C} C terminus regulate VDI. Further, we present data and a model showing how both modes of inactivation utilize the I-II linker as a blocking particle.

*Correspondence: gp2004@columbia.edu

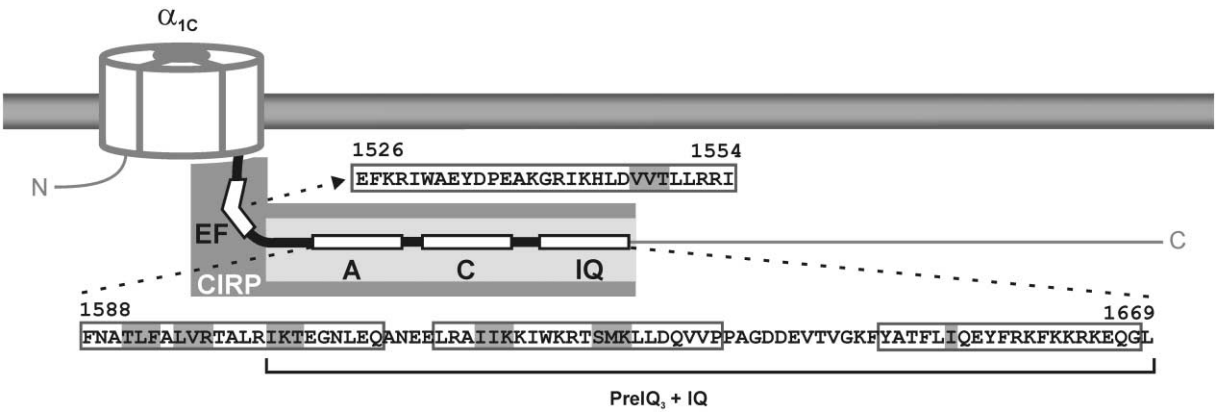

Figure 1. Schematic Diagram of α_{1C}, with EF, Peptide A, Peptide C, IQ, PreIQ$_3$+IQ Region, and Sequence Details Indicated

The EF hand (Babitch, 1990), peptide A and peptide C (Pitt et al., 2001), IQ (Zühlke et al., 1999), and PreIQ$_3$+IQ region (Erickson et al., 2003) have been previously identified. Amino acids mutated for biochemical and functional studies are shaded. The darker gray box denotes the CIRP (amino acids 1507–1669), and the lighter gray box indicates the aa 1558–1669 construct.

Results

Isolation and Purification of the Ca^{2+}-Sensing Complex

To investigate the function of the Ca^{2+}-sensing apparatus responsible for CDI, we attempted to obtain material suitable for in vitro analyses. To optimize chances that we would be able to infer that results from biochemical analyses on a part of the channel were applicable to the understanding of integrated channel function, we established as a primary criterion that the material needed to be soluble in detergent-free conditions. The major assumption underlying this principle derived from the observation that CDI and VDI utilize common molecular determinants (Cens et al., 1999). This implied that the sensing apparatus should function as a semi-independent entity, transmitting its information to the downstream inactivation machinery in order to accelerate the rate of inactivation compared to that produced by voltage alone. Thus, the Ca^{2+}-sensing apparatus should be able to be isolated as a soluble component. We therefore co-expressed CaM and a Hisx6-tagged fragment of the α_{1C} C terminus in bacteria and purified the resultant complex via metal affinity chromatography. Initially, we obtained no material with or without CaM co-expression in attempts to express aa 1558–1669 (Figures 1 and 2A), a segment that contained all of the C-terminal domains reported to contribute to CaM interaction, starting after EF and continuing through IQ (Mouton et al., 2001; Pate et al., 2000; Peterson et al., 1999; Pitt et al., 2001; Romanin et al., 2000; Zühlke et al., 1999). This result was consistent with the reduced expression of α_{1C} seen when EF was deleted (Zhou et al., 1997). We therefore tested whether the presence of EF, a putative CDI signal-transducing element (Peterson et al., 2000), was necessary with a construct containing amino acids 1507–1669. This fragment extended from the end of IVS6 through IQ (Figure 1A) and corresponded closely to the CI region (CIR) that can transfer robust CDI from α_{1C} to α_{1E} (de Leon et al., 1995). Indeed, an α_{1C} subunit truncated after aa 1669 displayed CDI that was indistinguishable from a full-length wt α_{1C} subunit (Figure 2B). While we could express this CIR peptide (CIRP), we only obtained insoluble material in the absence of CaM co-expression (Figure 2A). Further, when we purified this material from the bacterial pellet under several denaturing conditions, we were unable to detect binding to CaM, even after the removal of the denaturants (data not shown). This shows that, in the absence of CaM co-expression, CIRP does not attain the critical structure necessary for CaM interaction. With CaM co-expression, we obtained a soluble CIRP/CaM complex in a detergent-free buffer in which the components copurified in a 1:1 stoichiometric ratio (Figure 2A).

The CIRP/CaM complex underwent a significant Ca^{2+}-

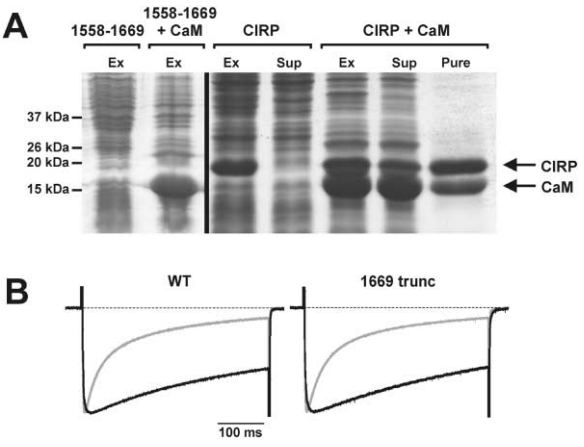

Figure 2. CaM and CIRP Form a Stable Complex

(A) Coomassie-stained gel showing purification of the CIRP/CaM complex. Lanes 1 and 2, crude bacterial extract showing absence of expression of the 1558–1669 construct, with or without CaM co-expression. Lanes 3 and 4, in the absence of CaM co-expression, CIRP is present in the crude extract (Ex) but not in the supernatant (Sup) after a 100,000 × g ultracentrifugation. Lanes 5 and 6, co-expression with CaM results in soluble CIRP. Lane 7, purified CIRP/CaM complex.

(B) Representative I_{Ba} (black) and I_{Ca} (gray) traces recorded from α_{1C} wt and α_{1C} truncated after aa 1669 (1669 trunc) expressed in *Xenopus* oocytes during 400 ms test pulses of V_h from −90 to +20 mV.

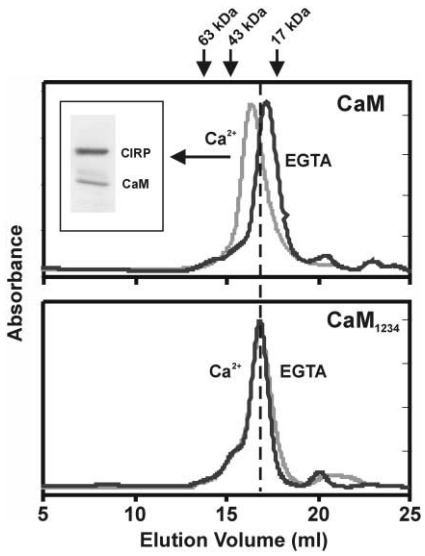

Figure 3. CaM and CIRP Form a Ca^{2+} Sensor

Gel filtration analysis of the CIRP/CaM (top) and CIRP/CaM_{1234} (bottom) complex in 10 μM Ca^{2+} (gray) or 5 mM EGTA (black). The dashed line represents the peaks for CIRP/CaM_{1234}. Inset shows a Coomassie-stained gel of the peak fraction (CIRP/CaM) collected off of the gel filtration column.

dependent conformational change. The complex migrated over a gel filtration column in the presence of Ca^{2+} as a single species with an apparent M_w of about 40 kDa, the predicted M_w for the sum of CaM plus CIRP (Figure 3 and Table 1). CIRP also associated with apoCaM. Since free $[Ca^{2+}]_i$ in *E. coli* is maintained at ~90 nM (Gangola and Rosen, 1987), the ability to isolate a complex indicated that the interaction between CaM and CIRP was stable at levels approximating free $[Ca^{2+}]_i$ in resting cells. Moreover, the CIRP/CaM complex migrated on the gel filtration column in the presence of EGTA as a single peak, albeit slower than with added Ca^{2+} (Figure 3 and Table 1). The change in elution volume between the conditions far exceeded the difference attributable to the apparent M_w of four Ca^{2+} ions, indicating that the CIRP/CaM complex underwent a significant conformational change while remaining associated over the entire dynamic range of $[Ca^{2+}]_i$.

We also examined the interaction of CIRP with CaM_{1234}, a CaM mutant in which all four EF hands are unable to bind Ca^{2+} that acts as a dominant negative to block CDI (Alseikhan et al., 2002; Peterson et al., 1999; Pitt et al., 2001). Migration of this complex on a gel filtration column was unaffected by Ca^{2+}, and the elution profiles were virtually indistinguishable from that of the wt CaM-containing complex when run in EGTA (Figure 3 and Table 1). This result suggested that the structure of CIRP/CaM_{1234} complex in either Ca^{2+} or EGTA resembled closely the CIRP/apoCaM complex, offering a biochemical confirmation of the proposed mechanism for the dominant-negative effects of CaM_{1234} upon the CDI Ca^{2+}-sensing apparatus.

Table 1. Summary of Gel Filtration Data

Complex	Ca^{2+}	EGTA
Wild-type/CaM	16.0	17.2
Wild-type/CaM_{1234}	16.8	16.8
WT_{EF}	16.1	17.1
I/A	16.2	17.1

For each gel filtration profile shown in the figures, the peak in either 10 μM Ca^{2+} or 5 mM EGTA containing buffer is shown. The peak was detected with the AKTA Unicorn software. For internal consistency, data for each complex shown in the Figures and in the Table were obtained from a single preparation. Data were first collected in the presence of Ca^{2+}. The peak fraction was collected and then reapplied to the column after pre-equilibration with EGTA. Each complex was purified at least three times with similar results.

Identification of Domains that Contribute to apoCaM Tethering

The ability to obtain a stable, pure CIRP/apoCaM complex allowed us to probe the determinants of apoCaM tethering, focusing on the ~110 amino acid domain between EF and IQ, which contains peptides A, C, and IQ (Figure 1). We first analyzed the contribution of peptide A by alanine scanning mutagenesis of ^{1591}TLF^{1593}, ^{1595}LVR^{1597}, and ^{1602}IKT^{1604} (designated TLF_A, LVR_A, and IKT_A, respectively) in CIRP (Figure 1A). The IKT_A sequence sits at the amino-terminal border of the recently proposed apoCaM binding region, while the TLF_A and LVR_A sequences lie farther N-terminal (Erickson et al., 2003). All three mutants displayed markedly decreased affinity for apoCaM; almost all of the CIRP present in the crude lysate did not copurify with CaM and was lost after ultracentrifugation at 100,000 × g, while the co-expressed CaM remained soluble (Figure 4A). The small amount of IKT_A that remained soluble eluted in the void volume on the gel filtration column (exclusion limit = 1300 kDa), suggesting that it was highly aggregated (Figure 4B). To confirm that the defect was a reduced affinity for apoCaM and not only for Ca^{2+}/CaM, we also co-expressed TLF_A with CaM_{1234} and again found almost no soluble CIRP (data not shown). The result with TLF_A and LVR_A indicated that components responsible for the apoCaM tethering domain extend more proximal than the recently proposed $PreIQ_3$ border (Erickson et al., 2003).

Having extended the boundary for apoCaM interaction, we then tested whether the essential requirement of EF both for expression of CDI (Zühlke and Reuter, 1998) and to obtain soluble CaM/CIRP complex (Figure 2A) implied a contribution to apoCaM tethering. Functional analysis of EF chimeras, in which residues were changed to their counterparts in α_1 subunits that display less robust CDI, had pinpointed ^{1547}VVT^{1549} as critical for CDI (Peterson et al., 2000). We therefore tested whether mutation to the α_{1B} sequence MFE (VVT_{EF}) disrupted apoCaM interaction. We obtained soluble VVT_{EF} CIRP/CaM complex from which CaM copurified with CIRP, showing that this mutation does not affect CaM interaction (Figures 4A and 4B and see below). In conjunction with the requirement for EF as demonstrated in Figure 2B, these data suggested that the EF hand helps stabilize and is a necessary part of the CIRP/CaM complex rather than contributing to CaM interaction.

Peptide C has also been reported to play a major role in apoCaM tethering (Erickson et al., 2003; Mouton et al., 2001; Pate et al., 2000; Pitt et al., 2001), but we found

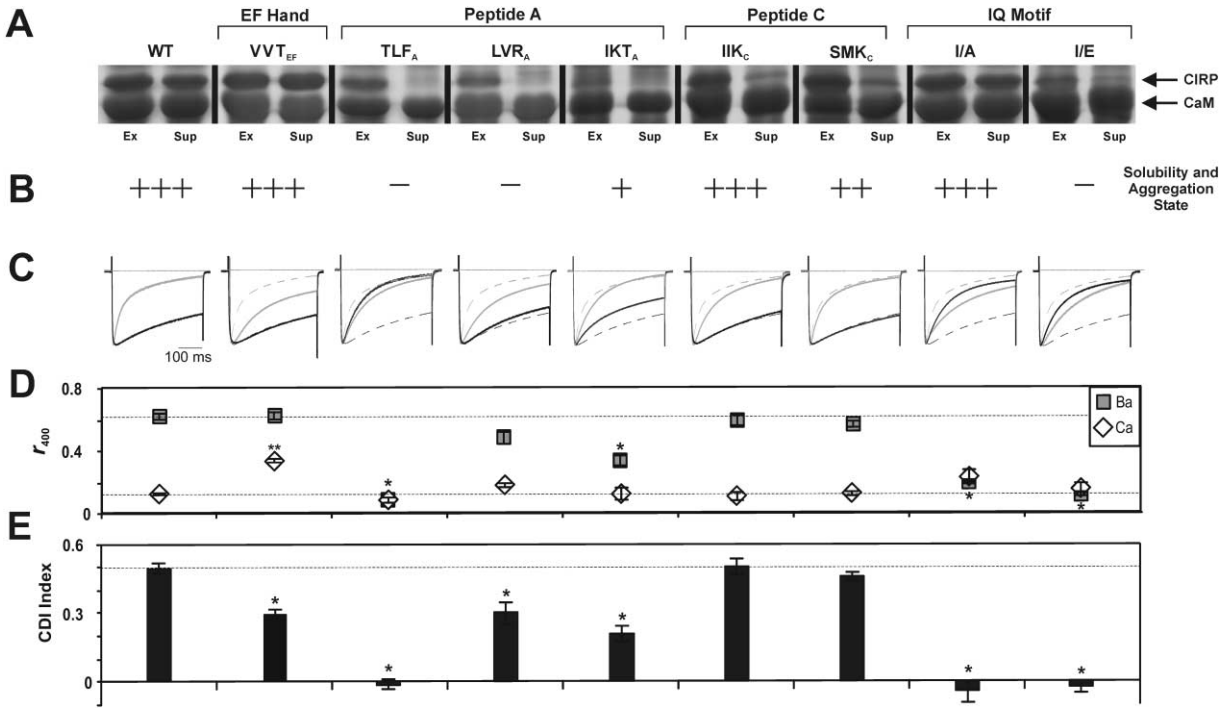

Figure 4. Mutations in Peptide A, Peptide C, and IQ Affect CIRP/CaM Complex Formation, CDI, and VDI

(A) Coomassie-stained gel of various mutant complexes, showing the region where CIRP and CaM appear. For each pair, the whole-cell extract (Ex) and high-speed supernatant (Sup) are shown.

(B) Semiquantitative assessment of effects of the mutations shown in (A): +++, the purified material migrated as a single species of ~40 kDa apparent M_W on the gel filtration column in a Ca^{2+}-containing buffer; ++, >50% of the purified material was aggregated (apparent M_W > 1300 kDa); +, all of the purified material was aggregated; −, no soluble material was obtained for purification. Each mutant complex was expressed and purified at least twice.

(C) Representative I_{Ba} (black) and I_{Ca} (gray) traces recorded from α_{1C} wt (dashed) and mutants (solid) expressed in *Xenopus* oocytes during 400 ms test pulses of V_h from −90 to +20 mV.

(D) Residual fraction of currents (r_{400}) remaining at the end of the test pulses for Ba^{2+} and Ca^{2+} (n = 5–11, *p < 0.01 versus wt for Ba^{2+}, **p < 0.01 for Ca^{2+}).

(E) CDI index for wt and mutants (n = 5–11, *p < 0.01 versus wt).

a more modest contribution compared to peptide A. When we analyzed the effects of mutating key residues in peptide C, ^{1618}IIK^{1620} and ^{1627}SMK^{1629}, to alanines (designated IIK_C and SMK_C, respectively), we observed that a significant portion of the CIRPs did not copurify with CaM and was lost after ultracentrifugation. Some material remained soluble and, after purification, IIK_C migrated as a single species on the gel filtration column (Figures 4A and 4B and data not shown). Although this confirmed results showing peptide C's contribution to apoCaM tethering (Erickson et al., 2003), the more modest effects of the mutations fit well with predictions based on the Ca^{2+} dependence of CaM interaction with peptide C (Pitt et al., 2001).

We next explored IQ, as its role in apoCaM tethering has been controversial (Erickson et al., 2003; Pitt et al., 2001). We tested the mutations I1654A (I/A) and I1654E (I/E), since they have nearly identical effects on channel inactivation (Zühlke et al., 1999), but only I/E affected the interaction of an IQ peptide for CaM (Zühlke et al., 2000). Consistent with those results, the I/A mutation had no obvious effect upon CIRP/CaM complex formation, while almost none of the I/E mutant CIRP coexpressed with CaM was recovered in the supernatant after ultracentrifugation (Figures 4A and 4B). The result with I/E confirmed a recent report that IQ contributes to apoCaM tethering (Erickson et al., 2003). However, the maintenance of apoCaM interaction with I/A conflicted with the proposal (Erickson et al., 2003) that accelerated voltage-dependent inactivation (VDI), as seen with I/A (Zühlke et al., 1999), is a functional hallmark of channels that have lost apoCaM tethering.

Mutations that Affect CaM Interaction Either Accelerate or Slow VDI

Identification of several apoCaM tethering mutants throughout CIRP allowed us to test formally the hypothesis that disruption of apoCaM tethering accelerates VDI and additionally to assess the effects of these mutants upon CDI. We generated the same mutations tested above in full-length α_{1C} for expression in *Xenopus* oocytes along with accessory subunits β_1 and $\alpha_2\delta$. Representative I_{Ba} and I_{Ca} traces recorded during 400 ms test pulses to +20 mV from $V_h = -90$ mV are shown in Figure 4C. Pooled data were analyzed using the ratio of the current values at 400 ms and at the initial peak (residual current at 400 ms, or r_{400} [Zühlke et al., 1999]) as an index of inactivation (Figure 4D). We then calculated the CDI index as the difference between the r_{400} for I_{Ba} and the r_{400} for I_{Ca} (Figure 4E).

Table 2. Kinetics of I_{Ba} and I_{Ca} Inactivation at +20 mV

Barium Time Constants of Inactivation

Channel	τ_1 (ms)	p Value versus Wild-Type τ_1	τ_2 (ms)	p Value versus Wild-Type τ_2	Fraction of I_1 (%)	n
Wild-type	1069 ± 53.9	–	154 ± 10.0	–	72.3 ± 3.27	7
VVT_{EF}	1129 ± 85.1	0.56	250 ± 14.2	<0.01	55.1 ± 1.51	7
TLF_A	110 ± 6.33	<0.01	–	<0.01*	–	8
LVR_A	667 ± 81.8	<0.01	147 ± 16.5	0.71	65.2 ± 4.36	4
IKT_A	387 ± 36.3	<0.01	60.8 ± 5.27	<0.01	61.3 ± 3.02	6
IIK_C	1046 ± 101	0.82	253 ± 23.8	<0.01	72.4 ± 2.27	7
SMK_C	983 ± 85.9	0.43	185 ± 5.74	0.03	78.0 ± 2.10	4
I/A	134 ± 7.22	<0.01	–	0.05*	–	5
I/E	110 ± 4.30	<0.01	–	<0.01*	–	12

Calcium Time Constants of Inactivation

Channel	τ_1 (ms)	p Value versus Wild-Type τ_1	τ_2 (ms)	p Value versus Wild-Type τ_2	Fraction of I_1 (%)	n
Wild-type	186 ± 2.10	–	31.8 ± 3.09	–	52.0 ± 2.10	6
VVT_{EF}	532 ± 13.9	<0.01	94.8 ± 3.65	<0.01	43.5 ± 2.12	6
TLF_A	176 ± 12.2	0.59	–	<0.01*	–	4
LVR_A	300 ± 22.2	<0.01	55.0 ± 2.75	<0.01	69.6 ± 5.39	5
IKT_A	189 ± 24.2	0.90	56.1 ± 5.02	<0.01	55.9 ± 3.21	7
IIK_C	317 ± 17.9	<0.01	52.7 ± 1.85	<0.01	54.9 ± 2.10	5
SMK_C	192 ± 9.20	0.06	29.8 ± 1.41	0.57	47.8 ± 3.11	9
I/A	201 ± 10.9	0.24	–	<0.01*	–	6
I/E	190 ± 6.82	0.67	–	<0.01*	–	11

During a 400–2000 ms test pulse to +20 mV, inactivation time constants were estimated by fitting the inactivating component of the current trace to the following equation: $I = I_o + I_1 \exp(-t/\tau_1) + I_2 \exp(-t/\tau_2)$, except the TLF_A, I/A, and I/E mutants, which were best fit by a single exponential. I_o is the residual current amplitude at equilibrium; I_1 and I_2 are the amplitudes of the current components. Fraction of I_1 is percent contribution of τ_1 to total inactivation, calculated as $I_1/(I_1 + I_2)$. Values are means ± SEM. n = number of tested oocytes.
*Mutant τ_1 versus wt τ_2

Consistent with our ability to generate a soluble CIRP/CaM complex with the VVT_{EF} mutation (Figures 4A and 4B), we observed that the VVT_{EF} mutant still displayed robust CDI (Figures 4C–4E), as measured by the CDI index, although it was significantly reduced compared to wt. This reduction was almost entirely due to a marked increase of the r_{400} for Ca^{2+}. Thus, the CDI defect caused by this mutation in EF is more likely attributable to inefficient signal transduction between the Ca^{2+} sensor and the inactivation machinery, consistent with EF's proposed role in signal transduction (Peterson et al., 2000), rather than a defect in apoCaM tethering.

Mutations within peptide A that disrupted apoCaM tethering showed varied effects upon VDI and CDI. The TLF_A and IKT_A mutations reduced CDI by decreasing the r_{400} for Ba^{2+} while having no appreciable effect upon the r_{400} for Ca^{2+} (r_{400} for wt = 12% ± 0.63%; for TLF_A = 9.4% ± 1.3%; for IKT_A = 11% ± 4.1%; p = .11 and p = .89 compared to wt, for TLF_A and IKT_A, respectively). In contrast, the LVR_A mutation modestly decreased the r_{400} for Ba^{2+} (r_{400} for wt = 62% ± 2.1% and for LVR = 48% ± 3.9%, p = 0.022) and modestly increased the r_{400} for Ca^{2+} (r_{400} for LVR = 18% ± 1.5%, p = 0.012) compared to wt (Figure 4D). As a result, CDI was reduced. Thus, all three apoCaM tethering mutants in the peptide A region reduced CDI, but the loss of apoCaM tethering did not consistently cause isolated and dramatic acceleration of VDI.

Mutations in peptide C that affected apoCaM tethering did not accelerate VDI. The Ba^{2+} r_{400} values for IIK_C and SMK_C were indistinguishable from wt (Figures 4C–4E), although further analysis indicated that VDI was slowed (see below and Table 2). As the r_{400} values for Ca^{2+} were equally unaffected, the CDI index for each of the peptide C mutants was similar to wt.

We obtained data consistent with previous results (Zühlke et al., 1999) for mutations within IQ, showing that the r_{400} for Ba^{2+} is nearly equal to the r_{400} for Ca^{2+} for both IQ mutants (Figures 4C and 4D). The net effect was a complete loss of CDI (Figure 4E). These data demonstrated that the I/A mutation caused accelerated VDI even when apoCaM interaction remained intact (Figure 4A). Thus, the I/A mutation along with the peptide C mutations showed that loss of apoCaM tethering is neither necessary nor sufficient for producing accelerated VDI.

Analysis of the kinetics of I_{Ba} inactivation for the mutants that affected CaM interaction with α_{1C} demonstrated that the CIRP/CaM complex does contribute to regulation of VDI. Parameters derived from fits of the decay phase of I_{Ba} were determined for wt and for the mutants during test pulses for 400–2000 ms from V_h = −90 mV to V_h = +20 mV and are shown in Table 2. The decay phase of I_{Ba} for the wt channel was best fit with two exponentials. Several of the mutants showed significant differences from wt, although the effects upon VDI were not consistent. The peptide A mutations, which had the most pronounced effect upon CaM interaction, decreased both τ_1 and τ_2. In fact, the decay phase of TLF_A, which displayed the fastest I_{Ba} inactivation, could be fit well with a single exponential. In contrast, the peptide C mutants, which have a moderate effect upon CaM interaction, increased τ_2 and had little effect upon τ_1. Particularly revealing were the results for the

IQ mutants, as the I_{Ba} decay phases for both I/A and I/E could be fit well with a single exponential. Since I/A did not affect CaM interaction with CIRP, the changes in inactivation kinetics for the IQ mutations likely do not result from alterations in CaM interaction (see below).

Ile1654 Couples the CIRP/CaM Complex to the Inactivation Machinery

Since the CIRP/CaM complex influenced both CDI and VDI, we hypothesized that it must control a common component of the inactivation machinery. The cytoplasmic linker between domains I and II on α_{1C} forms a putative blocking particle that mediates both CDI and VDI (Cens et al., 1999; Stotz et al., 2000), and analysis of chimeras between α_{1C} and α_{1S} had also implicated the I-II loop in CDI (Adams and Tanabe, 1997), making it an attractive candidate for the common component of the CDI and VDI signal transduction pathways. We therefore tested whether the CIRP/CaM complex interacted with the I-II loop. As shown in Figure 5A, the complex specifically bound to the I-II loop in a Ca^{2+}-dependent manner. Even with a large excess input of CIRP/CaM complex in this GST pull-down assay, we detected almost no interaction with the I-II loop in EGTA-containing buffer. We also tested the interaction of the VVT_{EF} mutant complex with the I-II loop, as the slower I_{Ca} inactivation kinetics suggested this mutant might be deficient in signal transduction between the Ca^{2+} sensor and the inactivation machinery. While the mutant complex also showed a Ca^{2+}-dependent interaction with the I-II loop, it appeared weaker than wt (Figure 5A).

We then considered whether the decreased interaction seen with the VVT_{EF} mutant complex was due either to the direct or indirect alteration of critical contact sites or to the inability of the VVT_{EF} mutant complex to undergo the Ca^{2+}-dependent confirmation conducive to interaction. To test between these possibilities, we analyzed the migration of the purified VVT_{EF} CIRP/CaM complex on the gel filtration column. As shown in Figure 5B (and Table 1), it retained the Ca^{2+}-dependent shift in mobility, demonstrating intact Ca^{2+} binding and preserved ability to undergo the Ca^{2+}-dependent conformational change. Thus, the defect in the interaction of the VVT_{EF} complex with the I-II loop appears to involve direct or indirect changes in the necessary contact sites.

To further probe the signal transduction pathway between the Ca^{2+} sensor and the inactivation machinery, we next focused on Ile1654, as further analysis of the effects of the I/A mutation on both I_{Ca} and I_{Ba} kinetics suggested that Ile1654 serves as a critical link between the CIRP/CaM complex and action of the blocking particle. The first indication came from an attempt to understand the mutant's similar kinetics of inactivation for Ba^{2+} and Ca^{2+} (Figures 4C–4E), as that result implied either that the channel's inactivation sensor could not distinguish between Ba^{2+} and Ca^{2+} or that the coupling between the sensor and the inactivation machinery was diminished. To test between these possibilities, we examined whether the I/A mutation perturbs the Ca^{2+} sensor. As shown in Figure 5C (and Table 1), the I/A CIRP/CaM complex, like the VVT_{EF} complex, also retained the Ca^{2+}-dependent shift in mobility on the gel filtration column, demonstrating intact Ca^{2+} binding and preserved

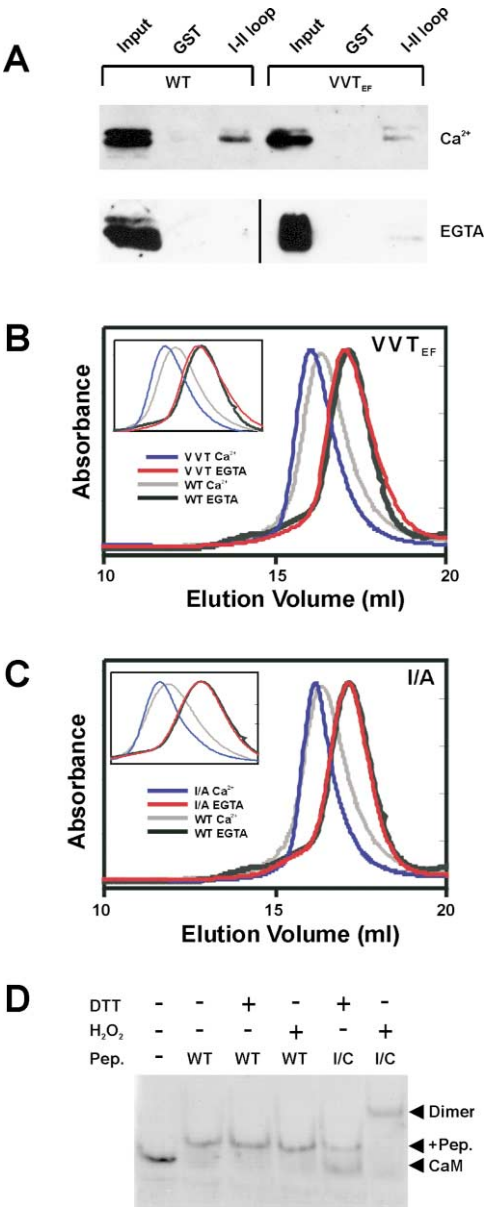

Figure 5. Ile1654 and EF Link the CIRP/CaM Complex to the Inactivation Machinery

(A) Immunoblot with an anti-6xHis antibody of a GST pull-down assay with GST-I-II loop or GST control and purified 6xHis CIRP/CaM or purified 6xHis CIRP/CaM with the VVT_{EF} mutation. In the top panel, 1 mM Ca^{2+} was added to binding and wash buffers and the input lane shows 100% of the added CIRP/CaM complexes. In the bottom panel, binding and wash buffers contained 2 mM EGTA with no added Ca^{2+}, and the input lane shows 25% of the added CIRP/CaM complexes. Ponceau staining of the nitrocellulose filters confirmed that the fusion proteins were equally loaded.

(B) Gel filtration analysis of the VVT_{EF} CIRP/CaM complex overlaid on the wt traces.

(C) Gel filtration analysis of the I/A CIRP/CaM complex overlaid on the wt traces.

(D) Coomassie-stained nondenaturing, nonreducing polyacrylamide gel of CaM with or without added IQ peptide (wt or I/C) in the presence or absence of hydrogen peroxide or DTT, showing that the I1654 position remains exposed when IQ is bound to CaM.

ability to undergo the Ca^{2+}-dependent conformational change. Support for the alternative uncoupling hypothesis was then found in the reconsideration of two previous results. First, I/A channels revealed an overt Ca^{2+}-dependent facilitation (Zühlke et al., 1999) that is masked in wt channels by a competing inactivation process (Zühlke et al., 2000). Second, dominant-negative CaM mutants, which lock the sensor in the apoCaM conformation (Figure 2C), failed to affect either I_{Ba} or I_{Ca} in I/A channels (Zühlke et al., 1999). Interpretation of those results in this context is consistent with ineffective or uncoupled signal transduction between the Ca^{2+} sensor and the inactivation machinery.

For I1654 to couple the sensor to the inactivation machinery, it must be accessible when CaM is bound to IQ. Previous analysis of an extensive set of I1654 mutations hinted at this possibility, identifying a requirement for a bulky hydrophobic side chain in that position for expression of CDI (Zühlke et al., 2000). Therefore, we probed the accessibility of the I1654 side chain when CaM was bound to IQ by exploring the redox potential of the well-characterized I/C mutant, which largely spares CDI and has minimal effects upon CaM interaction with IQ (Zühlke et al., 2000). In a gel shift analysis of CaM plus the I/C mutant IQ peptide, we observed a slower migrating species if the preformed complex was subjected to oxidizing conditions (Figure 5D) but not reducing conditions. Since there are no other cysteine residues in the mutant IQ peptide and none within CaM, this must result from a disulfide bond formed between two mutated IQ peptides. Further, since we did not visualize any bands when the same amount of this icosapeptide was run in the absence of CaM, under oxidizing or reducing conditions (data not shown), the slower migrating species must represent a $(CaM/peptide)_2$ dimer, formed by the single disulfide bond between the two cysteine residues on the IQ peptide. Dimer formation is specific to the presence of the Cys residue, as we tested nine other mutant IQ peptides that did not contain Cys in addition to the wt peptide shown, and none of them produced the supershift seen with I/C peptide. Thus, these data showed that the isobutyl group on I1654 must be exposed when bound to CaM, consistent with the possibility that it provides the critical hydrophobic contacts that couple the CIRP/CaM complex to the inactivation machinery.

Discussion

A Unified Model for VDI and CDI

Isolation and characterization of the Ca^{2+} sensor and recognition of its interaction with the putative blocking particle allowed us to propose a model to explain how CDI and VDI utilize the same molecular determinants for inactivation (Figure 6A). While interpretation of our data could lead to several independent models, we propose one to stimulate further study. In its role as the putative signal transducer (Peterson et al., 2000), we hypothesize that EF sits between the CaM binding domain and the I-II loop and prevents the I-II loop, either directly or indirectly, from blocking the channel. Although we do not detect a Ca^{2+}-independent interaction between the CIRP/CaM complex and the I-II loop, we hypothesize its presence to explain slow Ca^{2+}-independent inactivation (VDI). We attribute our inability to detect this interaction to the absence of other critical components in our assay. Candidate components include the $Ca_V\beta$ subunit, which has a prominent role in regulating the kinetics of inactivation (Catterall, 2000), and/or portions of the other intracellular loops, some of which have known roles in Ca^{2+} channel inactivation (Geib et al., 2002). The other stabilizing interactions in the resting state are the hydrophobic contracts formed by Ile1654. Together, these prevent the I-II loop from occluding the pore. In the absence of Ca^{2+}, the proximity of EF to IVS6 allows the voltage-dependent conformational changes in the transmembrane segments to be translated to EF and slowly relieve this inhibition, permitting the I-II loop to initiate inactivation. Ca^{2+} accelerates inactivation by inducing a Ca^{2+}/CaM-dependent conformational change in the Ca^{2+}-sensor apparatus, removing the Ile1654-mediated inhibition. Not only does this disinhibit the I-II loop, but Ca^{2+} also allows a productive interaction of the CIRP/CaM complex with the I-II loop to accelerate inactivation.

The actions of the I/A mutant (Figure 6B) can then be understood as the loss of the Ile1654-mediated inhibition; substitution of the isobutyl group on isoleucine for the smaller methyl group of alanine causes loss of hydrophobic contacts necessary to link the CIRP/CaM complex to the inactivation machinery. Since the CIRP/CaM complex no longer hinders the I-II loop, the response to a voltage-dependent conformational change, in the absence of Ca^{2+}, proceeds rapidly. In the presence of Ca^{2+}, rapid inactivation occurs even as the Ca^{2+} sensor undergoes a futile Ca^{2+}-dependent conformational change. While it may be premature to assign specific conformational changes to individual rate constants, it is interesting to note that the kinetics of inactivation in both Ba^{2+} and Ca^{2+} for the I/A mutant are best described by a single exponential rather than the two exponentials required for wt. Perhaps the loss of one rate constant reflects the uncoupling process.

Further, this model can also explain the slower CDI observed with the VVT_{EF} mutant as a consequence of an inefficient interaction between the CIRP/CaM complex and the I-II loop, as suggested by the data presented in Figure 5. Finally, this model also allows us to predict that those mutations that markedly decreased the affinity for apoCaM, for which we were unable to obtain suitable material for biochemical analysis, would affect inactivation by altering the Ca^{2+} sensor's conformation and/or coupling with EF.

Inherent in this model is that measures of VDI and CDI would be difficult to separate experimentally, as attempts to affect one process may invariably alter the other. Previous assessments of CDI have used parameters measuring differences in inactivation kinetics between conditions with Ca^{2+}-containing solutions and solutions containing another permeant divalent cation such as Ba^{2+}. Thus, the interpretation of the effects of certain mutations in Figure 4 on CDI needs to consider that the primary process altered may have been VDI, thus precluding the expression of CDI even if the mechanisms for Ca^{2+} responsiveness remain intact.

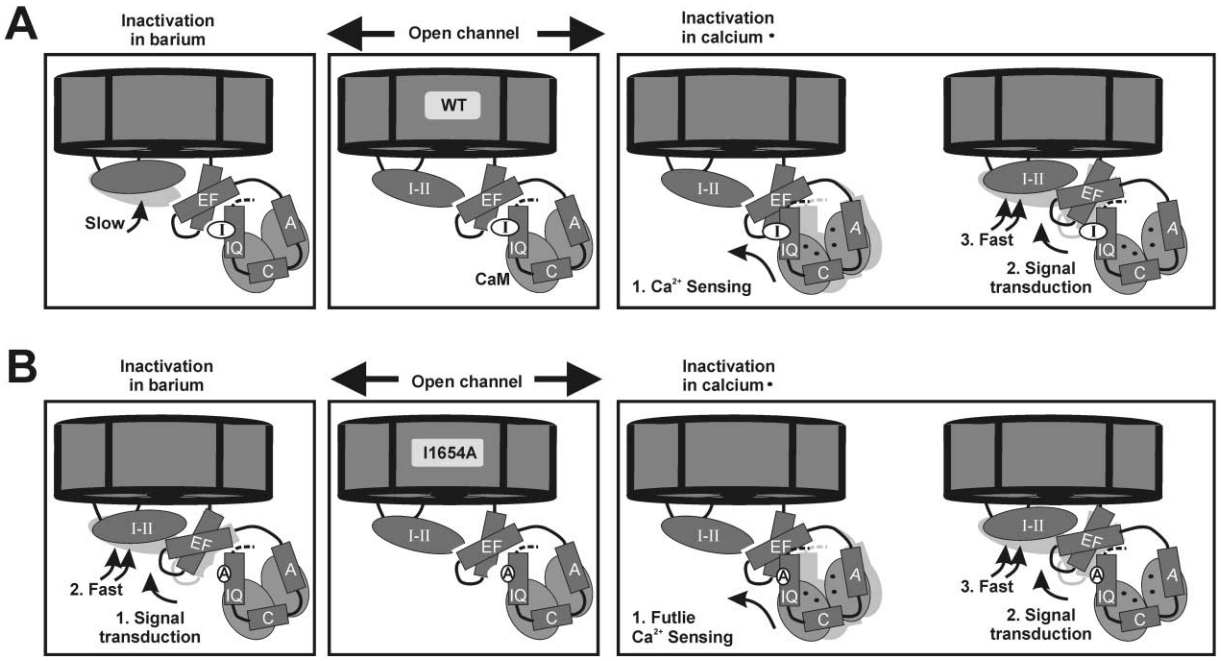

Figure 6. Model for CDI and VDI

(A) Model showing mechanism of inactivation for wt channel. Open channel is shown in the middle box. Voltage induces a slow conformational change that allows the I-II loop to interact with the pore (left). Ca^{2+} influx causes a Ca^{2+}/CaM-induced conformational change that then relieves the EF-mediated inhibition of the I-II loop, allowing an accelerated interaction of the I-II loop with the pore (right).

(B) Model showing mechanism of uncoupling due to I1654A mutation. Loss of the bulky isobutyl side chain at aa 1654 uncouples the Ca^{2+} sensor from EF, relieving the EF-mediated inhibition of the I-II loop. In Ba^{2+} (left) or Ca^{2+} (right), inactivation proceeds rapidly.

CaM Tethering and Effector Domains Are Inseparable

CaM is pictured as interacting with the A-IQ domains in both its Ca^{2+}-loaded and Ca^{2+}-free states. Indeed, a primary finding here is that the α_{1C} C-terminal apoCaM tethering domains and Ca^{2+}/CaM effector domains that regulate CDI are inseparable. Analysis of CIRP mutants showed that the peptide A region, the peptide C region, and IQ not only contribute to apoCaM tethering but also contribute to Ca^{2+}/CaM effector functions. The identical features—loss of CDI and disruption in CaM interaction—that defined the IQ motif as a Ca^{2+}/CaM effector domain were characteristic of mutations in the regions analyzed in this study. Previous models for CDI based upon assignment of apoCaM tethering or Ca^{2+}/CaM effector domains to specific regions within the proximal portion of the α_{1C} C terminus need to be reassessed.

The disparities between the results obtained with smaller peptides (Erickson et al., 2003; Pitt et al., 2001; Tang et al., 2003) and those obtained with the entire proximal portion of the α_{1C} C terminus (data from this study) likely reflect altered binding properties displayed by the smaller peptides, which may only contribute a part of the binding energy inherent to the whole CaM binding site. For example, we observed moderate effects of the peptide C mutations upon CaM interaction with CIRP, in contrast to the results obtained with nearly identical peptide C mutations analyzed with FRET two-hybrid mapping (Erickson et al., 2003). Consistent with our findings, the peptide C mutations also had moderate effects upon inactivation kinetics; the effects of the mutations analyzed by Erickson et al. (2003) on inactivation were not assessed.

The generation of a stable, soluble complex between CaM and this fragment of the α_{1C} terminus inclusive of all the regions previously identified as essential for CDI was a critical step in establishing this model. Purification of the complex and its use in a cell-free system offered several advantages over the previous assays used for analyzing the interaction between CaM and α_{1C} C-terminal fragments. First, we were able to assess the interaction between CaM and its α_{1C} binding target at the two extremes of $[Ca^{2+}]_i$. Second, this approach avoided spurious interactions due to coincident subcellular targeting of CaM and the α_{1C} C terminus mutants that can take place with in vivo assessment of protein-protein interactions. Indeed, we have observed that certain fragments of the α_{1C} C terminus abnormally aggregate in subcellular compartments when expressed in mammalian cell culture (data not shown). Third, we assessed direct binding between α_{1C} C terminus mutants and CaM, avoiding the complexities and constraints of an interpretation based on interactions between protein tags such as GFP. Finally, our material is pure and aggregation-resistant in a detergent-free system. This represents clearing of a significant hurdle in the biochemical characterization of this interaction, as certain fragments of α_{1C} have proven difficult to express in bacteria as soluble material in the absence of detergent (De Waard et al., 1995; Pitt et al., 2001). This allowed us to avoid the concerns that our protein is improperly folded, or that it could act as a nidus for nonspecific interactions or

protein aggregation, which would preclude accurate assessment of binding.

This new model for CaM interaction with the α_{1C} C terminus contributes to the expanding repertoire used by CaM to recognize target proteins. A canonical CaM recognition site is an unlikely contributor here, as the CaM binding pocket in the α_{1C} C terminus extends over at least 80 amino acids. The formation of a CaM binding site from the contribution of multiple, noncontiguous regions on the SK channel provides a basis for comparison (Schumacher et al., 2001), and analysis of CaM interaction with the *B. anthracis* edema factor (Drum et al., 2000) may also offer insight, as the contact region between the two proteins extends over 6000 Å (Liddington, 2002). It is interesting to note that canonical 1-8-14 and 1-5-10 CaM binding sequences (Rhoads and Friedberg, 1997) originally identified in edema factor do not contribute to CaM contact sites when viewed in the crystal structure (Drum et al., 2002). Whether peptide A, peptide C, or the IQ motif will suffer the same fate remains to be determined, but this observation underscores the problems in trying to predict CaM contact sites from sequence analysis.

Experimental Procedures

Construction of cDNA Plasmids

The plasmid encoding the α_{1C} subunit used for expression in *Xenopus* oocytes, pCARDHE, was a generous gift of W. Sather (U. of Colorado). Mutagenesis was performed with QuikChange (Stratagene) on an EcoRV-XmaI fragment encoding the α_{1C} C terminus that had been subcloned into the pSP70 shuttle vector. After mutagenesis, the entire fragment was sequenced and then subcloned into pCARDHE. The plasmid encoding the α_{1C} 1507–1669 fragment (CIRP) and 1558–1669 fragment were generated by amplifying the appropriate DNA by PCR with primers containing endonuclease restriction sites. Products were digested with the appropriate enzymes and ligated into pET28a+ (Novagen). Mutations were generated with QuikChange. The CaM wt and CaM_{1234} expression plasmids were generated by subcloning bovine CaM (wt) or a mutated rat CaM (CaM_{1234}) into pSGC02 (Ghosh and Lowenstein, 1996).

Electrophysiology

In vitro transcription and microinjection into *Xenopus* oocytes of α_{1C} and the auxiliary Ca^{2+} channel subunits β_1 (Ruth et al., 1989) and $\alpha_2\delta$ (Singer et al., 1991) were performed generally as previously described (Zühlke et al., 2000). In brief, in vitro transcription was performed using mMessage mMachine (Ambion) after linearizing the cDNA vector with the appropriate enzyme. 46 nl of a cRNA mixture, containing 10–50 fmol/μl of α_{1C} and 5–10 fmol/μl of β_1 and $\alpha_2\delta$ subunits, was microinjected into stage V or VI *Xenopus* oocytes, which were then kept at 17°C–19°C in a sterile Barth's medium supplemented with penicillin and streptomycin (Specialty Media) and used for recordings 3–7 days later. Before recording whole-cell I_{Ba} or I_{Ca}, oocytes were injected with 25–50 nl of 100 mM BAPTA solution (pH 7.4) to minimize contaminating Ca^{2+}-activated Cl^- currents. During I_{Ba} recordings, oocytes were constantly superfused with a solution containing 40 mM $Ba(OH)_2$, 50 mM NaOH, 1 mM KOH, and 10 mM HEPES (adjusted to pH 7.4 with methanesulfonic acid). To evoke I_{Ca}, the bath solution was switched to a solution containing $Ca(NO_3)_2$ instead of $Ba(OH)_2$. Recordings were performed with a standard two-electrode voltage clamp configuration using an oocyte clamp OC-725C amplifier (Warner Instrument Corp.) connected through a Digidata 1322A A/D interface (Axon Instruments) to a personal computer. Ionic currents were filtered at 1 kHz by an integral 4 pole Bessel filter and sampled 10 kHz and analyzed with Clampfit 8.1.

Protein Expression and Purification

The α_{1C} 1507–1669 with and without the CaM or CaM_{1234} expression plasmids were transformed into BL-21 cells by electroporation. Cells were grown to an $OD_{600} = 0.3$ and then expression was induced with the addition of IPTG for 72 hr at 16°C. Cell extracts were prepared by passage through a French pressure cell. The lysates were then centrifuged at 100,000 × g for 90 min, and the supernatants were then applied to Talon metal affinity resin (Clontech). The CaM/α_{1C} 1507–1669 complex was eluted with 250 mM imidazole, aliquoted, and stored at −20°C in 25% glycerol for further use. Gel filtration was performed over a Superdex 200 HR 10/30 column on an AKTA FPLC (Amersham Biosciences) in 500 mM NaCl, 5 mM imidazole, 20 mM Tris, 25% glycerol (pH 7.5), supplemented with either 10 μM $CaCl_2$ or 5 mM EGTA. Generation of the GST fusion protein containing the I-II intracellular loop has previously been described (Pitt et al., 2001).

GST Pull-Down Assay

The GST I-II loop fusion protein and the GST control were bound to glutathione sepharose 4B (Amersham) and washed extensively, and samples were then run on SDS-PAGE for quantification. To remaining aliquots of both bound GST I-II loop fusion protein and GST, wt, or mutant CIRP complex was incubated for 60 min at 25°C in 150 mM NaCl, 50 mM Tris, 0.1% Triton (pH 7.4) supplemented either with 1 mM Ca^{2+} or 2 mM EGTA. The bound complexes were then washed extensively in the same buffer, eluted in SDS sample buffer, and separated by SDS-PAGE. Proteins were transferred to nitrocellulose, and immunoblotting was performed with a polyclonal anti-6xHis antibody (Covance).

Gel Shift Analysis

Calmodulin, purified as described (Pitt et al., 2001), was allowed to interact with an IQ peptide containing the I/C mutation (Zühlke et al., 2000), and the complex was then run on a nondenaturing, nonreducing polyacrylamide gel (15%) as described (Zühlke et al., 1999), in the presence of 10 mM dithiothreitol or 0.1% hydrogen peroxide, as indicated. Calmodulin was visualized by Coomassie blue staining.

Acknowledgments

We thank Gareth Tibbs for his many helpful and insightful discussions. This work was supported by NIH R01 HL71165 to G.S.P.

Received: October 16, 2003
Revised: December 12, 2003
Accepted: January 23, 2004
Published: March 3, 2004

References

Adams, B., and Tanabe, T. (1997). Structural regions of the cardiac Ca channel alpha subunit involved in Ca-dependent inactivation. J. Gen. Physiol. *110*, 379–389.

Alseikhan, B.A., DeMaria, C.D., Colecraft, H.M., and Yue, D.T. (2002). Engineered calmodulins reveal the unexpected eminence of Ca2+ channel inactivation in controlling heart excitation. Proc. Natl. Acad. Sci. USA *99*, 17185–17190.

Babitch, J. (1990). Channel hands. Nature *346*, 321–322.

Bernatchez, G., Talwar, D., and Parent, L. (1998). Mutations in the EF-hand motif impair the inactivation of barium currents of the cardiac alpha1C channel. Biophys. J. *75*, 1727–1739.

Budde, T., Meuth, S., and Pape, H.C. (2002). Calcium-dependent inactivation of neuronal calcium channels. Nat. Rev. Neurosci. *3*, 873–883.

Catterall, W.A. (2000). Structure and regulation of voltage-gated Ca2+ channels. Annu. Rev. Cell Dev. Biol. *16*, 521–555.

Cens, T., Restituito, S., Galas, S., and Charnet, P. (1999). Voltage and calcium use the same molecular determinants to inactivate calcium channels. J. Biol. Chem. *274*, 5483–5490.

de Leon, M., Wang, Y., Jones, L., Perez-Reyes, E., Wei, X., Soong, T.W., Snutch, T.P., and Yue, D.T. (1995). Essential Ca(2+)-binding motif for Ca(2+)-sensitive inactivation of L-type Ca2+ channels. Science *270*, 1502–1506.

De Waard, M., Witcher, D.R., Pragnell, M., Liu, H., and Campbell,

K.P. (1995). Properties of the alpha 1-beta anchoring site in voltage-dependent Ca2+ channels. J. Biol. Chem. *270*, 12056–12064.

Drum, C.L., Yan, S.Z., Sarac, R., Mabuchi, Y., Beckingham, K., Bohm, A., Grabarek, Z., and Tang, W.J. (2000). An extended conformation of calmodulin induces interactions between the structural domains of adenylyl cyclase from *Bacillus anthracis* to promote catalysis. J. Biol. Chem. *275*, 36334–36340.

Drum, C.L., Yan, S.Z., Bard, J., Shen, Y.Q., Lu, D., Soelaiman, S., Grabarek, Z., Bohm, A., and Tang, W.J. (2002). Structural basis for the activation of anthrax adenylyl cyclase exotoxin by calmodulin. Nature *415*, 396–402.

Erickson, M.G., Liang, H., Mori, M.X., and Yue, D.T. (2003). FRET two-hybrid mapping reveals function and location of L-type Ca(2+) channel CaM preassociation. Neuron *39*, 97–107.

Gangola, P., and Rosen, B. (1987). Maintenance of intracellular calcium in *Escherichia coli*. J. Biol. Chem. *262*, 12570–12574.

Geib, S., Sandoz, G., Cornet, V., Mabrouk, K., Fund-Saunier, O., Bichet, D., Villaz, M., Hoshi, T., Sabatier, J.M., and De Waard, M. (2002). The interaction between the I–II loop and the III–IV loop of Cav2.1 contributes to voltage-dependent inactivation in a beta-dependent manner. J. Biol. Chem. *277*, 10003–10013.

Ghosh, S., and Lowenstein, J.M. (1996). A multifunctional vector system for heterologous expression of proteins in *Escherichia coli*. Expression of native and hexahistidyl fusion proteins, rapid purification of the fusion proteins, and removal of fusion peptide by Kex2 protease. Gene *176*, 249–255.

Liang, H., DeMaria, C.D., Erickson, M.G., Mori, M.X., Alseikhan, B.A., and Yue, D.T. (2003). Unified mechanisms of Ca(2+) regulation across the Ca(2+) channel family. Neuron *39*, 951–960.

Liddington, R.C. (2002). Anthrax: a molecular full nelson. Nature *415*, 373–374.

Mouton, J., Feltz, A., and Maulet, Y. (2001). Interactions of calmodulin with two peptides derived from the c-terminal cytoplasmic domain of the Ca(v)1.2 Ca2+ channel provide evidence for a molecular switch involved in Ca2+-induced inactivation. J. Biol. Chem. *276*, 22359–22367.

Pate, P., Mochca-Morales, J., Wu, Y., Zhang, J.Z., Rodney, G.G., Serysheva, I.I., Williams, B.Y., Anderson, M.E., and Hamilton, S.L. (2000). Determinants for calmodulin binding on voltage-dependent Ca2+ channels. J. Biol. Chem. *275*, 39786–39792.

Peterson, B.Z., DeMaria, C.D., Adelman, J.P., and Yue, D.T. (1999). Calmodulin is the Ca2+ sensor for Ca2+-dependent inactivation of L-type calcium channels. Neuron *22*, 549–558.

Peterson, B.Z., Lee, J.S., Mulle, J.G., Wang, Y., de Leon, M., and Yue, D.T. (2000). Critical determinants of Ca(2+)-dependent inactivation within an EF-hand motif of L-type Ca(2+) channels. Biophys. J. *78*, 1906–1920.

Pitt, G.S., Zuhlke, R.D., Hudmon, A., Schulman, H., Reuter, H., and Tsien, R.W. (2001). Molecular basis of calmodulin tethering and Ca2+-dependent inactivation of L-type Ca2+ channels. J. Biol. Chem. *276*, 30794–30802.

Rhoads, A.R., and Friedberg, F. (1997). Sequence motifs for calmodulin recognition. FASEB J. *11*, 331–340.

Romanin, C., Gamsjaeger, R., Kahr, H., Schaufler, D., Carlson, O., Abernethy, D.R., and Soldatov, N.M. (2000). Ca(2+) sensors of L-type Ca(2+) channel. FEBS Lett. *487*, 301–306.

Ruth, P., Rohrkasten, A., Biel, M., Bosse, E., Regulla, S., Meyer, H.E., Flockerzi, V., and Hofmann, F. (1989). Primary structure of the beta subunit of the DHP-sensitive calcium channel from skeletal muscle. Science *245*, 1115–1118.

Schumacher, M.A., Rivard, A.F., Bachinger, H.P., and Adelman, J.P. (2001). Structure of the gating domain of a Ca2+-activated K+ channel complexed with Ca2+/calmodulin. Nature *410*, 1120–1124.

Singer, D., Biel, M., Lotan, I., Flockerzi, V., Hofmann, F., and Dascal, N. (1991). The roles of the subunits in the function of the calcium channel. Science *253*, 1553–1557.

Stotz, S.C., Hamid, J., Spaetgens, R.L., Jarvis, S.E., and Zamponi, G.W. (2000). Fast inactivation of voltage-dependent calcium channels. A hinged-lid mechanism? J. Biol. Chem. *275*, 24575–24582.

Tang, W., Halling, D.B., Black, D.J., Pate, P., Zhang, J.Z., Pedersen, S., Altschuld, R.A., and Hamilton, S.L. (2003). Apocalmodulin and ca(2+)calmodulin-binding sites on the ca(v)1.2 channel. Biophys. J. *85*, 1538–1547.

Zhou, J., Olcese, R., Qin, N., Noceti, F., Birnbaumer, L., and Stefani, E. (1997). Feedback inhibition of Ca2+ channels by Ca2+ depends on a short sequence of the C terminus that does not include the Ca2+ -binding function of a motif with similarity to Ca2+-binding domains. Proc. Natl. Acad. Sci. USA *94*, 2301–2305.

Zühlke, R.D., and Reuter, H. (1998). Ca2+-sensitive inactivation of L-type Ca2+ channels depends on multiple cytoplasmic amino acid sequences of the alpha1C subunit. Proc. Natl. Acad. Sci. USA *95*, 3287–3294.

Zühlke, R.D., Pitt, G.S., Deisseroth, K., Tsien, R.W., and Reuter, H. (1999). Calmodulin supports both inactivation and facilitation of L-type calcium channels. Nature *399*, 159–162.

Zühlke, R.D., Pitt, G.S., Tsien, R.W., and Reuter, H. (2000). Ca2+-sensitive inactivation and facilitation of L-type Ca2+ channels both depend on specific amino acid residues in a consensus calmodulin-binding motif in the alpha 1C subunit. J. Biol. Chem. *275*, 21121–21129.